Fermion-Parity-Based Computation and Its Majorana-Zero-Mode Implementation

Campbell K. McLauchlan[1] and Benjamin Béri[1,2]

[1]*DAMTP, University of Cambridge, Wilberforce Road, Cambridge CB3 0WA, United Kingdom*

[2]*T.C.M. Group, Cavendish Laboratory, University of Cambridge, J.J. Thomson Avenue, Cambridge CB3 0HE, United Kingdom*

(Received 27 October 2021; accepted 29 March 2022; published 5 May 2022)

Majorana zero modes (MZMs) promise a platform for topologically protected fermionic quantum computation. However, creating multiple MZMs and generating (directly or via measurements) the requisite transformations (e.g., braids) pose significant challenges. We introduce fermion-parity-based computation (FPBC): a measurement-based scheme, modeled on Pauli-based computation, that uses efficient classical processing to virtually increase the number of available MZMs and which, given magic state inputs, operates without transformations. FPBC requires all MZM parities to be measurable, but this conflicts with constraints in proposed MZM hardware. We thus introduce a design in which all parities are directly measurable and which is hence well suited for FPBC. While developing FPBC, we identify the "logical braid group" as the fermionic analog of the Clifford group.

DOI: 10.1103/PhysRevLett.128.180504

Pauli-based computation (PBC) is an intriguing measurement-based alternative to the circuit model of quantum computing [1]. By performing only a minimal number of adaptive Pauli measurements on "magic state" inputs, PBC allows one to virtually expand the number of qubits in a quantum computer and forego the need to perform Clifford gates [2], at the cost of efficient classical processing. While PBC is formulated for qubits, quantum computing can also use fermionic modes [3]. Fermionic quantum computing is better suited to certain tasks, a notable example being many-electron, including quantum chemistry, simulations [3,4]. For the fermionic hardware, Majorana zero modes (MZMs) are a promising option, as they offer topological protection of quantum information [4–9].

In this Letter, we formulate fermion-parity-based computation (FPBC), a fermionic counterpart of PBC, and propose a MZM hardware design well-suited to its implementation. En route, we identify the "logical braid group" as the group of all Clifford-like fermionic gates. For MZM computing, FPBC does not just mean fewer MZMs: it is a new computational model, distinct from the circuit model of previous measurement-based approaches [9–13], that eliminates the need to generate braiding and other Clifford-like transformations [8–15], and thus avoids the associated overheads [13,16,17].

A key requirement for FPBC is to be able to measure potentially complicated strings of MZMs. We find that configuration constraints present obstacles to this in existing MZM designs. Our design, based on top-transmon ingredients [18–21], is free of such constraints. Furthermore, unlike circuit-based computing in existing designs [4,9–13,21], FPBC with our design uses no ancilla MZMs. The only remaining limitation is locality, as we shall explain.

Fermionic quantum computing and logical braids.— Consider $2n$ Majorana operators $\gamma_j = \gamma_j^\dagger$ $(j = 1, \ldots, 2n)$ with anticommutator $\{\gamma_j, \gamma_k\} = 2\delta_{jk}$. These $2n$ modes have total fermion parity $\Gamma_{2n} = i^n \prod_{j=1}^{2n} \gamma_j$. Let $\mathrm{Maj}(m)$ denote the group of Majorana strings generated by $\gamma_1, \ldots, \gamma_m$ and the phase factor i, and $\overline{\mathrm{Maj}}(m)$ denote the subgroup of $\mathrm{Maj}(m)$ that commutes with Γ_{2n}. We call the Hermitian elements of $\overline{\mathrm{Maj}}(m)$ fermion parity operators; FPBC will be based on their adaptive measurements.

To develop FPBC, we first consider fermionic quantum computing in the circuit model, and then, analogously to PBC [1,22], show how FPBC can simulate it. We consider fermionic circuits based on the universal gate set $\{W_{4,abcd} = \exp[i(\pi/4)\gamma_a\gamma_b\gamma_c\gamma_d], T_{2,ab} = \exp[(\pi/8)\gamma_a\gamma_b]\}$ [3]. Note that noncommuting W_4 operators can generate all possible gates of the form $W_{2k,i_1 i_2 \ldots i_{2k}} = \exp[\pm i^{k+1}(\pi/4)\gamma_{i_1}\gamma_{i_2}\ldots\gamma_{i_{2k}}]$ (including braid operators $W_{2,ab}$ [7,23–25]). This is because $W_{4,abcd}$ is a "logical braid" between γ_a and $i\gamma_b\gamma_c\gamma_d$, the latter being a "logical Majorana" relative to γ_a (i.e., a parity-odd, Hermitian Majorana string anticommuting with γ_a [26]), and hence can send $W_{2k} \mapsto W_{2k\pm 2}$ under conjugation. Because of this observation we refer to the group generated by the W_4 as the logical braid group and its elements, including all W_{2k}, as logical braids. Under conjugation, W_4 gates map between strings in $\mathrm{Maj}(2n)$ [31]; they are Clifford-like. Indeed, logical braids are the only parity-preserving unitaries with this property [32].

A key insight for FPBC is that a T_2 gate can be implemented via a "magic state gadget." Here, we describe this procedure using a dense encoding [7] of magic states, which is more suitable for our fermionic hardware (cf. below) and a more efficient use of quantum resources [4]. To implement t T_2 gates, assume we have a separate

　

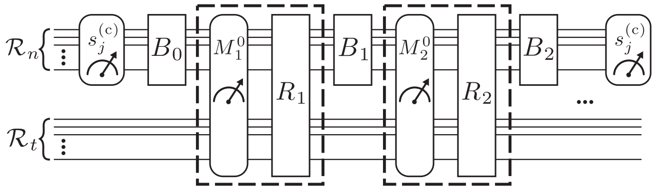

FIG. 1. An arbitrary fermionic circuit C on register $\mathcal{R}_n$, to be simulated by FPBC. The T_2 gates are enacted via magic state gadgets (dashed boxes), with magic states encoded in register $\mathcal{R}_t$. The gadgets involve a two-register fermion parity measurement M_j^0 and a measurement-dependent logical braid R_j. C involves t uses of the gadget, interspersed with logical braids B_i, and ends with the measurement of all $s_j^{(c)}$. Dummy measurements of all $s_j^{(c)}$ are appended to the start of C.

register $\mathcal{R}_t$ of $2t+2$ Majoranas with its own conserved parity Γ_{2t+2}. Define two sets of operators in $\overline{\mathrm{Maj}}(2t+2)$: $\{X_1, X_2, \ldots, X_t\}$ and $\{s_j = i\gamma_{2j-1}\gamma_{2j} | j = 1, \ldots, t\}$, obeying $\{s_j, X_j\} = 0$ (for all j) and $[s_{j'}, X_j] = [X_{j'}, X_j] = [s_{j'}, s_j] = 0$ ($j' \neq j$). Then let register $\mathcal{R}_t$ be in the state $|\psi^{(t)}\rangle = T_{2,12}T_{2,34}\ldots T_{2,2t-1\ 2t}|\psi^X\rangle$, where $|\psi^X\rangle$ is the $+1$ eigenstate of all X_j operators. Thus, the register contains t magic states densely encoded into $2t+2$ Majoranas. The gate $T_{2,ab} = \exp[(\pi/8)\gamma_a\gamma_b]$ can then be applied to Majoranas a, b in a separate register $\mathcal{R}_n$ with its own conserved parity, using the procedure or "gadget" (shown in Fig. 1): $\mathcal{M}_{j,ab} = R_j \Pi^{m_j}_{is_j\gamma_a\gamma_b}$, for $j \in \{1, \ldots, t\}$, enacted on both registers. Here, $\Pi^{m_j}_{is_j\gamma_a\gamma_b}$ is the projector representing the measurement of $is_j\gamma_a\gamma_b$ with outcome m_j, and $R_j = \{\exp[(\pi/4)\gamma_b\gamma_a]\}^{(1+m_j)/2}\exp[(\pi/4)\gamma_a\gamma_b X_j]$ is a measurement-dependent logical braid.

Magic states can be distilled from multiple approximate copies with logical braids and measurements, using magic state distillation [4,31,35,36]—this is one of the leading candidates for preparing high-fidelity magic states in Majorana-based architectures, and thereby for achieving fault-tolerant, universal quantum computation [4,7,9,27,37,38]. Much work has been devoted to optimizing its resource cost [39–42] and finding alternatives that can also be used to prepare magic states [43,44].

Fermion-parity-based computation.—By performing adaptive fermion parity measurements only on $\mathcal{R}_t$ initialized in state $|\psi^{(t)}\rangle$, and efficient classical processing, FPBC can simulate an arbitrary fermionic circuit C on $\mathcal{R}_n$. Without loss of generality, we take C to act on $\mathcal{R}_n$ initialized in the $+1$ eigenstate of all $s_j^{(c)}$ [$j = 1, \ldots, n$; (c) indicates $\mathcal{R}_n$ operators], and that it uses $t = \mathrm{poly}(n)$ T_2 gates, interspersed with logical braids B_i (recall that T_2 gates and logical braids form a universal gate set [3]). C ends by measuring all $s_j^{(c)}$ on $\mathcal{R}_n$, i.e., sampling the output distribution. The bit string $\mathbf{b}$ of these final measurement results comprises the output of the circuit.

The first step towards simulating C by FPBC is to replace all T_2 gates with magic state gadgets. As shown in Fig. 1, C then involves logical braids B_i and R_i, fermion parity measurements (labeled M_i^0 for $i = 1, \ldots, t$) from the t uses of the gadget, and final $s_j^{(c)}$ measurements. We denote these final measurements $M_{t+j}^0 \equiv s_j^{(c)}$ ($j = 1, \ldots, n$). The next step is to eliminate all logical braids, by commuting the B_i and R_i to the end of the circuit, thereby updating $M_i^0 \mapsto M_i \in \overline{\mathrm{Maj}}[2(n+t+2)]$. Since the quantum state after the final measurement is discarded, the logical braids now have no effect on the output, and can be deleted. For what follows, we append a set of dummy measurements of all $s_j^{(c)}$ to the start of C, shown in Fig. 1, which have outcomes $+1$ on $\mathcal{R}_n$'s initial state, and define $M_{j-n} \equiv s_j^{(c)}$ for $j = 1, \ldots, n$. At this stage, either $[M_i, M_j] = 0$ or $\{M_i, M_j\} = 0$ for all i, j. We now show that one can limit the measurements to a mutually commuting set, thereby reducing the number needing to be performed and restricting the computation to $\mathcal{R}_t$. To achieve this, we go through the M_i sequence, starting with M_1, and, if we reach an i such that $\{M_i, M_j\} = 0$ for some $j < i$, we delete M_i and replace it with the logical braid

$$V(\lambda_i, \lambda_j) = \frac{\mathbb{1} + \lambda_i\lambda_j M_i M_j}{\sqrt{2}} = \exp\left(\frac{\pi}{4}\lambda_i\lambda_j M_i M_j\right), \quad (1)$$

where $\lambda_j = \pm 1$ is the measurement outcome of M_j and $\lambda_i = \pm 1$ is chosen uniformly at random. As in PBC [1,22], this simulates the measurement of M_i: $\{M_i, M_j\} = 0$ implies equal measurement probabilities $1/2$ for M_i, which is simulated by uniformly choosing λ_i at random, and since $\lambda_j M_j = \mathbb{1}$ on the premeasurement state, $V(\lambda_i, \lambda_j)$ produces the correct corresponding postmeasurement state. We then commute $V(\lambda_i, \lambda_j)$ past all $M_{l>i}$. Again, it can then be deleted. (Henceforth we leave the resulting updates of $M_{l>i}$ implicit.) For the final n measurements, if M_i is replaced by its corresponding $V(\lambda_i, \lambda_j)$, we include the classically randomly generated value of λ_i in $\mathbf{b}$.

Finally, we are left with a sequence of mutually commuting M_i. For $j \leq 0$ we still have dummy measurements $M_j = s_j^{(c)}$ and $\lambda_j = 1$, which completely specifies a basis of $\mathcal{R}_n$ (within a given parity sector). Hence, since $[M_1, M_j] = 0$ for all $j \leq 0$, we can restrict M_1 to $\mathcal{R}_t$ without changing its measurement distribution or postmeasurement state. We can then restrict M_2 to $\mathcal{R}_t$, since $[M_2, M_j] = 0$ for all $j \leq 1$, and so on. Doing this for all $M_{j>0}$ and then discarding $M_{j\leq 0}$, we thereby restrict the entire computation to $\mathcal{R}_t$. There are only t independent commuting parities (besides Γ_{2t+2}) on $\mathcal{R}_t$. Using efficient classical computation [45], one computes the outcomes for those M_j dependent on preceding M_i, and deletes them. The quantum part of the computation is thus reduced to the adaptive measurement

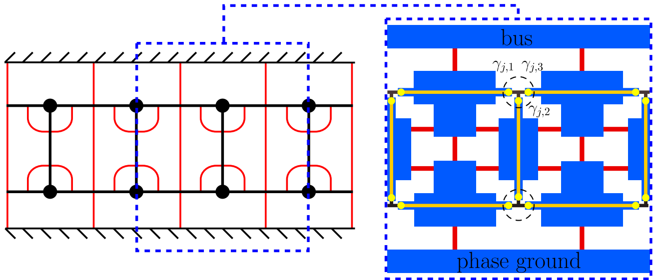

FIG. 2. Section of FPBC hardware. Left: top and bottom black dashed regions are superconducting plates—the bus and phase ground, respectively. Thick black lines correspond to nanowire-hosting superconducting islands while black dots indicate trijunctions between nanowires. The design may be continued to the right and left. Right: more detailed illustration of the region indicated. Superconducting plates and islands are shown in blue. Nanowires (yellow) host Majorana bound states (labeled 1, 2, and 3) at their ends, combining to form a single Majorana zero mode at each trijunction (dashed circles). In both panels, tunable Josephson junctions are indicated with red lines.

of $p \leq t$ mutually commuting parities on $\mathcal{R}_t$. The remaining entries in $\mathbf{b}$ (those not filled by the classically sampled λ_i) come from the outcomes of those $M_{j>t}$ that were not replaced by logical braids; via the process described above these outcomes are either measured explicitly or computed classically. Thus, assisted with poly(n)-time classical processing, we can sample from C's output distribution using FPBC.

FPBC hardware.—To perform FPBC, one needs hardware such that the fermion parities M_i on $\mathcal{R}_t$ are measurable. In existing MZM designs, one can measure only those M_i that meet certain configuration constraints. For example, in Majorana transmon setups [4,8,21,46] one has "readout islands" with a pair of MZMs on each, and only those M_i are measurable that feature no MZM without its readout-island pair. Magic state gadgets in these setups, however, require interisland logical braids and/or measurements, which can generate FPBCs with unmeasurable M_i [32]. (Subsequent braids may bring M_i to a measurable configuration; however, in typical setups, and for large t, only for a vanishingly small proportion of M_i does just a constant-in-t number of such braids suffice [32]).

We introduce a design (sketched in Fig. 2) that is free of such configuration constraints. The core ingredients and the corresponding physical considerations are based on Refs. [20,21]. The MZMs appear at trijunctions between Majorana bound states at the ends of spin-orbit nanowires on superconducting islands [5,47–60]. The islands are connected via tunable Josephson junctions (JJs) to other islands and, for some islands, also to one of two superconducting plates, called the bus and phase ground. This entire system is enclosed within a transmission line resonator. As we next explain, this has a parity-dependent resonance frequency, which allows one to measure the M_i via dispersive readout [15,18,20,46,61,62]. [The similar parity dependence of the transmon ground state can be used to implement (approximate) T_2 gates [20,21] and hence to supply (noisy) magic states for distillation].

A JJ between superconductors a and b, with phases ϕ_a and ϕ_b of their superconducting order parameters, respectively, contributes a term $E_{J,ab}[1-\cos(\phi_a-\phi_b)]$ to the Hamiltonian [63], for some energy $E_{J,ab}$ that can be controlled by fluxes or electrostatic gates [21,64,65]. By tuning these control parameters, each JJ can thus be turned on or off, corresponding to Josephson energy $E_{J,ab}^{(\mathrm{on/off})}$, where $E_{J,ab}^{(\mathrm{on})} \gg E_{J,ab}^{(\mathrm{off})}$. The kth island has charging energy scale $E_{C,k} = e^2/2C_k$ for total capacitance C_k between island k and all other superconductors to which it is connected. We take $E_{J,ab}^{(\mathrm{on/off})}$ to be of the same order of magnitude for all ab and similarly for $E_{C,k}$ across all k. In what follows, each island will be connected (directly or via a path of "on" JJs) to either the bus or phase ground; we call these bus-connected and ground-connected islands, respectively. We assume that the Josephson energy dominates for all islands, namely, that $E_{J,ak}^{(\mathrm{off})} \gtrsim E_{C,k}$ for all islands a, k with JJs connecting them. Given this, and that $E_{J,ak}^{(\mathrm{on})}/E_{C,k} \gg E_{J,bl}^{(\mathrm{off})}/E_{C,l}$ (for all $a,k;b,l$ with JJs), any bus-connected (ground-connected) island has superconducting phase pinned to that of the bus (phase ground) [21]. Hence, we can view the entire system as having a single effective JJ between bus- and ground-connected subsystems. The corresponding Josephson and charging energies are E_J and E_C, respectively, associated with sums of ("off"-state) Josephson energies and capacitances between the bus- and ground-connected subsystems. We will take $E_J \gg E_C$, i.e., work in the transmon regime [18].

The jth trijunction has Hamiltonian [14,15,21,66]

$$V_{M,j} = \frac{E_M}{2}\sum_{a,b,c=1}^{3}\epsilon_{abc}A_{j,a}(i\gamma_{j,b}\gamma_{j,c}) = iE_M|\mathbf{A}_j|\gamma_{j,+}\gamma_{j,-}. \tag{2}$$

Here $\gamma_{j,1}$, $\gamma_{j,2}$, and $\gamma_{j,3}$ are the Majorana bound states at the ends of the nanowires at the jth trijunction and E_M is the overall trijunction energy scale. The $A_{j,a}$ include phase-dependent cosines encoding the 4π-periodic Josephson effect [5,67] (cf. the flux-dependent couplings of Refs. [15,21]) and $|\mathbf{A}_j|^2 = \sum_{a=1}^{3} A_{j,a}^2$. The coupling of the three Majorana bound states results in a MZM which we denote $\gamma_{j,0}$, and two more Majorana modes $\gamma_{j,+}$ and $\gamma_{j,-}$ encoding a nonzero-energy fermion [32].

We take $E_M \ll \hbar\Omega_0$, where $\Omega_0 \approx \sqrt{8E_JE_C}/\hbar$ sets the transmon level spacing [18]; the system is thus a top-transmon perturbed by the $V_{M,j}$ [32]. For low-lying levels, $V_{M,j}$ can be taken at zero bus-ground phase difference [21]. Without $V_{M,j}$, the effect of Majorana bound states is a contribution $(-1)^m\delta\varepsilon_m\mathcal{P}$ to the mth transmon level energy, where $\delta\varepsilon_m \propto \exp(-\sqrt{8E_J/E_C})$, and $\mathcal{P}$ is the joint fermion parity of Majorana bound states on bus-connected islands [21,32]. In considering $V_{M,j}$, we work with $E_M \gg \delta\varepsilon_m$ and to first order in $\delta\varepsilon_m/E_M$. This allows one to project $\mathcal{P}$ to $Q = P_-\mathcal{P}P_-^\dagger$, where $P_- = \prod_j P_{j,-}$ with $P_{j,-} = (1 - i\gamma_{j,+}\gamma_{j,-})/2$.

Dispersive readout thus measures Q. The only fermion operators contributing to Q are the $\gamma_{j,0}$, with $\gamma_{j,0}$ entering Q if and only if there are an odd number of bus-connected islands around trijunction j. With one bus-connected island at trijunction j, only the $\gamma_{j,a}$ on that island features in $\mathcal{P}$; then the projection gives $P_-\gamma_{j,a}P_-^\dagger = A_{j,a}\gamma_{j,0}/|\mathbf{A}_j|$ [32]. For three bus-connected islands at trijunction j, all three $\gamma_{j,a}$ feature in $\mathcal{P}$; we have $P_-(i\gamma_{j,a}\gamma_{j,b}\gamma_{j,c})P_-^\dagger = P_-(i\gamma_{j,0}\gamma_{j,+}\gamma_{j,-})P_-^\dagger = -\gamma_{j,0}$. With two bus-connected islands, trijunction j contributes a scalar factor to Q: $P_-(i\gamma_{j,a}\gamma_{j,b})P_-^\dagger = -\sum_c \epsilon_{abc}A_{j,c}/|\mathbf{A}_j|$. For a given configuration of bus- and ground-connected islands, and focusing on the lowest two transmon levels ($m = 0$, 1), Q can be measured via the shift

$$\omega_{\text{shift}} = \frac{C}{2}(\delta\varepsilon_1 + \delta\varepsilon_0) \prod_{\substack{j|1,2\ \text{islands} \\ \text{bus connected}}} \frac{A_{j,\alpha_j}}{|\mathbf{A}_j|} \tag{3}$$

in the resonator's resonance frequency upon flipping Q's eigenvalue. Here, C is a constant dependent on transmon and resonator parameters [32], the product runs over trijunctions around which one or two islands are bus connected, and α_j is set by the jth trijunction's bus-connected island configuration.

Arbitrary parity measurement.—The preceding discussion hints that our design allows for the measurement of any MZM parity M_i. We now explain this in detail. Since $\gamma_{j,0}$ features in Q when an odd number of islands surrounding it are bus connected, precisely those $\gamma_{j,0}$ that are endpoints of a path of bus-connected islands feature in Q (see Fig. 3). We convert this observation into the following prescription: Let M_i feature those $\gamma_{j,0}$ with j in some set S_{M_i}. Index the labels $j \in S_{M_i}$ with $k_j = 1, \ldots, |S_{M_i}|$ such that $k_{j'} < k_j$ if $\gamma_{j,0}$ is to the right of or directly below $\gamma_{j',0}$ [cf. Fig. 3(f)]. Pair the $\gamma_{j,0}$ with successive k_j (i.e., first with second, third with fourth, etc.) and, for each pair, draw the shortest clockwise path of islands between the two MZMs. We then connect all islands featuring in an odd (even) number of paths to the bus (phase ground).

The measurement configuration thus formed for M_i is realizable with the JJs indicated in Fig. 2. The shortest clockwise path between a MZM pair is one of five basic paths shown in Figs. 3(a)–3(e). A combination of these is realizable if there exists a path through "on" JJs from every bus-connected (ground-connected) island to the bus (phase ground), and only "off" JJs link bus-connected and ground-connected subsystems. In Fig. 3 we indicate how the JJs achieve this for each basic path. All pairs of basic paths are trivially realizable if we omit Path (e), since then no bottom-row horizontal island is bus connected, and bus-connected vertical islands are always adjacent to a bus-connected horizontal island. There are a further five pairs that include Path (e) [(e)(i) for $i = a, \ldots, e$] which all can be checked to be realizable. Hence so too are all measurement configurations produced by the prescription. A 12-MZM example is shown in Fig. 3(f).

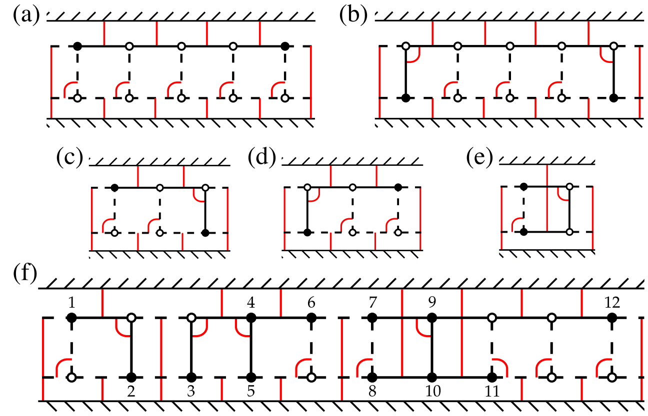

FIG. 3. The configuration for measuring any parity operator M is obtained by combining five basic paths [labeled (a)–(e)] of bus-connected islands; these are the shortest clockwise paths connecting pairs of MZMs. Paths (a)–(d) have variable length while Path (e) has a fixed length. Solid (dashed) lines in all panels indicate bus-connected (ground-connected) islands. Filled (unfilled) dots are MZMs that do (do not) feature in M. Only "on" Josephson junctions are indicated (red lines); others are omitted for clarity. As an example, Panel (f) shows the measurement configuration for a 12-MZM parity operator. The MZMs are indexed as in the main text and basic paths connect MZMs j and $j+1$ for odd j. When combining the basic paths, precisely those islands belonging to an odd number of paths are bus connected.

We thus find that implementing FPBC with our design could reduce the resource cost of MZM-based quantum computation. The required number of MZMs is reduced, both since the computation is restricted to $\mathcal{R}_t$ and since no ancilla MZMs are needed. We also reduce the total number of operations, by deleting all logical braids, and avoiding the overheads from braiding processes [68].

However, there is a residual limitation of locality in our design; it cannot be used for arbitrarily large registers $\mathcal{R}_t$. In ideal systems, this arises via the suppression of ω_{shift} with the number L of islands in the system. Since E_J and E_C characterize the effective JJ between bus- and ground-connected subsystems, they scale as $O(L)$ and $O(L^{-1})$, respectively, so we have $\delta\varepsilon_m \sim \exp(-cL)$ with c a constant [69]. ω_{shift} is further suppressed by a factor $A_{j,\alpha_j}/|\mathbf{A}_j|$ for every trijunction around which one or two islands are bus connected. Hence, increasing the size of $\mathcal{R}_t$ requires the ability to resolve increasingly small ω_{shift}. In realistic setups, larger and more complex systems may also incur more accidental features (e.g., material defects, accidental quantum dots). These may reduce coherence times and measurement fidelities [70–73], and pose challenges for calibrating parity measurements. However, one may be able to use techniques similar to those for mapping defect features and locations in transmon systems [70,74,75] to facilitate calibration, and reduce the number of defects with new materials techniques [73,76–79]. Additionally, in larger setups, more JJs allow for more quasiparticle poisoning events, which are not inhibited by a strong charging energy as they are in other designs [9]. However, these rates may still be small enough to be neglected on relevant timescales [80,81], and could be further reduced with quasiparticle traps [82,83].

Conclusion.—We have introduced fermion-parity-based computation, a low-resource-cost, measurement-based model of quantum computing with Majoranas, and have explained how it is able to simulate any fermionic quantum circuit. We introduced a MZM hardware design that is free of constraints on measurable operators, beyond those of locality, and hence is well suited to FPBC. We expect that a t-MZM FPBC, similarly to PBC [1], can be simulated by a $(t-k)$-MZM FPBC if supplemented by $\exp(k)$-time classical processing; thus with FPBC one could minimize the quantum resources needed for fermionic computation. To overcome the locality constraint, future work could consider how multiple copies of our setup might be used to measure larger fermion parities. We expect one could adapt existing work on transmon qubit-parity measurements [84–87] to our Majorana-transmon setup, wherein frequency shifts are produced only by (suitably generalized [28]) fermion parities. These larger setups could be made feasible by adapting transmon-based methods for improved measurements [88,89] and large device design and calibration [90–94]. One could also investigate our hardware design in the context of Majorana fermion codes [37,95], taking advantage of the large set of measurable operators.

We thank R. Jozsa for introducing us to PBC, and thank him and S. Strelchuk for useful discussions. This work was supported by an EPSRC Studentship, EPSRC Grant No. EP/S019324/1, and the ERC Starting Grant No. 678795 TopInSy.

[1] S. Bravyi, G. Smith, and J. A. Smolin, Phys. Rev. X **6**, 021043 (2016).
[2] D. Gottesman, Stabilizer codes and quantum error correction, Ph.D. thesis, CalTech, 1997.
[3] S. B. Bravyi and A. Y. Kitaev, Ann. Phys. (N.Y.) **298**, 210 (2002).
[4] T. E. O'Brien, P. Rożek, and A. R. Akhmerov, Phys. Rev. Lett. **120**, 220504 (2018).
[5] A. Y. Kitaev, Phys. Usp. **44**, 131 (2001).
[6] A. Y. Kitaev, Ann. Phys. (N.Y.) **321**, 2 (2006).
[7] S. D. Sarma, M. Freedman, and C. Nayak, npj Quantum Inf. **1**, 15001 (2015).
[8] D. Aasen, M. Hell, R. V. Mishmash, A. Higginbotham, J. Danon, M. Leijnse, T. S. Jespersen, J. A. Folk, C. M. Marcus, K. Flensberg, and J. Alicea, Phys. Rev. X **6**, 031016 (2016).
[9] T. Karzig, C. Knapp, R. M. Lutchyn, P. Bonderson, M. B. Hastings, C. Nayak, J. Alicea, K. Flensberg, S. Plugge, Y. Oreg, C. M. Marcus, and M. H. Freedman, Phys. Rev. B **95**, 235305 (2017).
[10] P. Bonderson, M. Freedman, and C. Nayak, Phys. Rev. Lett. **101**, 010501 (2008).
[11] H. Zheng, A. Dua, and L. Jiang, New J. Phys. **18**, 123027 (2016).
[12] R. W. Bomantara and J. Gong, Phys. Rev. B **101**, 085401 (2020).
[13] A. Tran, A. Bocharov, B. Bauer, and P. Bonderson, SciPost Phys. **8**, 91 (2020).
[14] J. Alicea, Y. Oreg, G. Refael, F. von Oppen, and M. P. A. Fisher, Nat. Phys. **7**, 412 (2011).
[15] B. van Heck, A. R. Akhmerov, F. Hassler, M. Burrello, and C. W. J. Beenakker, New J. Phys. **14**, 035019 (2012).
[16] M. Hell, J. Danon, K. Flensberg, and M. Leijnse, Phys. Rev. B **94**, 035424 (2016).
[17] C. Knapp, M. Zaletel, D. E. Liu, M. Cheng, P. Bonderson, and C. Nayak, Phys. Rev. X **6**, 041003 (2016).
[18] J. Koch, T. M. Yu, J. Gambetta, A. A. Houck, D. I. Schuster, J. Majer, A. Blais, M. H. Devoret, S. M. Girvin, and R. J. Schoelkopf, Phys. Rev. A **76**, 042319 (2007).
[19] J. A. Schreier, A. A. Houck, J. Koch, D. I. Schuster, B. R. Johnson, J. M. Chow, J. M. Gambetta, J. Majer, L. Frunzio, M. H. Devoret, S. M. Girvin, and R. J. Schoelkopf, Phys. Rev. B **77**, 180502(R) (2008).
[20] F. Hassler, A. R. Akhmerov, and C. W. J. Beenakker, New J. Phys. **13**, 095004 (2011).
[21] T. Hyart, B. van Heck, I. C. Fulga, M. Burrello, A. R. Akhmerov, and C. W. J. Beenakker, Phys. Rev. B **88**, 035121 (2013).
[22] M. Yoganathan, R. Jozsa, and S. Strelchuk, Proc. Math. Phys. Eng. Sci. **475**, 20180427 (2019).
[23] N. Read and D. Green, Phys. Rev. B **61**, 10267 (2000).
[24] D. A. Ivanov, Phys. Rev. Lett. **86**, 268 (2001).
[25] C. Nayak, S. H. Simon, A. Stern, M. Freedman, and S. Das Sarma, Rev. Mod. Phys. **80**, 1083 (2008).
[26] For other uses of logical Majoranas, see Refs. [27–30].
[27] Y. Li, Phys. Rev. A **98**, 012336 (2018).
[28] A. R. Akhmerov, Phys. Rev. B **82**, 020509(R) (2010).
[29] G. Goldstein and C. Chamon, Phys. Rev. B **86**, 115122 (2012).
[30] J. Behrends and B. Béri, Phys. Rev. Lett. **124**, 236804 (2020).
[31] S. Bravyi, Phys. Rev. A **73**, 042313 (2006).
[32] See Supplemental Material at http://link.aps.org/supplemental/10.1103/PhysRevLett.128.180504 for details on the logical braid group; measurements generated by FPBC; the resource cost of FPBC in other setups; and the top-transmon Hamiltonian, trijunctions and shift frequencies, which includes Refs. [33,34].

[33] S. Plugge, A. Rasmussen, R. Egger, and K. Flensberg, New J. Phys. **19**, 012001 (2017).
[34] J. F. Steiner and F. von Oppen, Phys. Rev. Research **2**, 033255 (2020).
[35] S. Bravyi and A. Kitaev, Phys. Rev. A **71**, 022316 (2005).
[36] A. M. Souza, J. Zhang, C. A. Ryan, and R. Laflamme, Nat. Commun. **2**, 169 (2011).
[37] D. Litinski and F. von Oppen, Phys. Rev. B **97**, 205404 (2018).
[38] M. Gau, R. Egger, A. Zazunov, and Y. Gefen, Phys. Rev. B **102**, 134501 (2020).
[39] S. Bravyi and J. Haah, Phys. Rev. A **86**, 052329 (2012).
[40] C. Jones, Phys. Rev. A **87**, 042305 (2013).
[41] J. Haah, M. B. Hastings, D. Poulin, and D. Wecker, Quantum **1**, 31 (2017).
[42] D. Litinski, Quantum **3**, 205 (2019).
[43] T. Karzig, Y. Oreg, G. Refael, and M. H. Freedman, Phys. Rev. X **6**, 031019 (2016).
[44] T. Karzig, Y. Oreg, G. Refael, and M. H. Freedman, Phys. Rev. B **99**, 144521 (2019).
[45] M. A. Nielsen and I. L. Chuang, *Quantum Computation and Quantum Information: 10th Anniversary Edition* (Cambridge University Press, Cambridge, England, 2010).
[46] T. B. Smith, M. C. Cassidy, D. J. Reilly, S. D. Bartlett, and A. L. Grimsmo, PRX Quantum **1**, 020313 (2020).
[47] Y. Oreg, G. Refael, and F. von Oppen, Phys. Rev. Lett. **105**, 177002 (2010).
[48] R. M. Lutchyn, J. D. Sau, and S. Das Sarma, Phys. Rev. Lett. **105**, 077001 (2010).
[49] J. Alicea, Rep. Prog. Phys. **75**, 076501 (2012).
[50] A. Das, Y. Ronen, Y. Most, Y. Oreg, M. Heiblum, and H. Shtrikman, Nat. Phys. **8**, 887 (2012).
[51] V. Mourik, K. Zuo, S. M. Frolov, S. R. Plissard, E. P. A. M. Bakkers, and L. P. Kouwenhoven, Science **336**, 1003 (2012).
[52] L. P. Rokhinson, X. Liu, and J. K. Furdyna, Nat. Phys. **8**, 795 (2012).
[53] M. T. Deng, C. L. Yu, G. Y. Huang, M. Larsson, P. Caroff, and H. Q. Xu, Nano Lett. **12**, 6414 (2012).
[54] C. Beenakker, Annu. Rev. Condens. Matter Phys. **4**, 113 (2013).
[55] P. Krogstrup, N. L. B. Ziino, W. Chang, S. M. Albrecht, M. H. Madsen, E. Johnson, J. Nygård, C. M. Marcus, and T. S. Jespersen, Nat. Mater. **14**, 400 (2015).
[56] S. M. Albrecht, A. P. Higginbotham, M. Madsen, F. Kuemmeth, T. S. Jespersen, J. Nygård, P. Krogstrup, and C. M. Marcus, Nature (London) **531**, 206 (2016).
[57] J. Chen, P. Yu, J. Stenger, M. Hocevar, D. Car, S. R. Plissard, E. P. A. M. Bakkers, T. D. Stanescu, and S. M. Frolov, Sci. Adv. **3**, e1701476 (2017).
[58] R. M. Lutchyn, E. P. A. M. Bakkers, L. P. Kouwenhoven, P. Krogstrup, C. M. Marcus, and Y. Oreg, Nat. Rev. Mater. **3**, 52 (2018).
[59] S. Vaitiekėnas, Y. Liu, P. Krogstrup, and C. Marcus, Nat. Phys. **17**, 43 (2021).
[60] K. Flensberg, F. von Oppen, and A. Stern, Nat. Rev. Mater. **6**, 944 (2021).
[61] K. Yavilberg, E. Ginossar, and E. Grosfeld, Phys. Rev. B **92**, 075143 (2015).
[62] D. I. Schuster, A. A. Houck, J. A. Schreier, A. Wallraff, J. M. Gambetta, A. Blais, L. Frunzio, J. Majer, B. Johnson, M. H. Devoret, S. M. Girvin, and R. J. Schoelkopf, Nature (London) **445**, 515 (2007).
[63] M. Tinkham, *Introduction to Superconductivity*, 2nd ed. (Dover Publications, New York, 2004).
[64] G. de Lange, B. van Heck, A. Bruno, D. J. van Woerkom, A. Geresdi, S. R. Plissard, E. P. A. M. Bakkers, A. R. Akhmerov, and L. DiCarlo, Phys. Rev. Lett. **115**, 127002 (2015).
[65] T. W. Larsen, K. D. Petersson, F. Kuemmeth, T. S. Jespersen, P. Krogstrup, J. Nygård, and C. M. Marcus, Phys. Rev. Lett. **115**, 127001 (2015).
[66] D. J. Clarke, J. D. Sau, and S. Tewari, Phys. Rev. B **84**, 035120 (2011).
[67] B. van Heck, F. Hassler, A. R. Akhmerov, and C. W. J. Beenakker, Phys. Rev. B **84**, 180502(R) (2011).
[68] Braids in a fermionic circuit do not increase the length of MZM strings in the resulting FPBC. They simply permute the MZMs in those strings. Hence, while their explicit implementation incurs some resource overhead [10,14–16] this cost is completely avoided in FPBC.
[69] One can include an extra Josephson junction directly connecting the bus and phase ground plates. For large Josephson energy, this results in the required $E_J \gg E_C$, thus allowing a smaller $E_{J,ab}^{(\mathrm{off})}$, and hence a smaller constant c.
[70] J. Lisenfeld, A. Bilmes, A. Megrant, R. Barends, J. Kelly, P. Klimov, G. Weiss, J. M. Martinis, and A. V. Ustinov, npj Quantum Inf. **5**, 105 (2019).
[71] S. E. de Graaf, L. Faoro, L. B. Ioffe, S. Mahashabde, J. J. Burnett, T. Lindström, S. E. Kubatkin, A. V. Danilov, and A. Y. Tzalenchuk, Sci. Adv. **6**, eabc5055 (2020).
[72] I. Siddiqi, Nat. Rev. Mater. **6**, 875 (2021).
[73] N. P. de Leon, K. M. Itoh, D. Kim, K. K. Mehta, T. E. Northup, H. Paik, B. S. Palmer, N. Samarth, S. Sangtawesin, and D. W. Steuerman, Science **372**, eabb2823 (2021).
[74] A. Bilmes, A. Megrant, P. Klimov, G. Weiss, J. M. Martinis, A. V. Ustinov, and J. Lisenfeld, Sci. Rep. **10**, 3090 (2020).
[75] G. Andersson, A. L. O. Bilobran, M. Scigliuzzo, M. M. de Lima, J. H. Cole, and P. Delsing, npj Quantum Inf. **7**, 15 (2021).
[76] A. Dunsworth, A. Megrant, C. Quintana, Z. Chen, R. Barends, B. Burkett, B. Foxen, Y. Chen, B. Chiaro, A. Fowler *et al.*, Appl. Phys. Lett. **111**, 022601 (2017).
[77] A. P. M. Place, L. V. H. Rodgers, P. Mundada, B. M. Smitham, M. Fitzpatrick, Z. Leng, A. Premkumar, J. Bryon, A. Vrajitoarea, S. Sussman *et al.*, Nat. Commun. **12**, 1779 (2021).
[78] A. Osman, J. Simon, A. Bengtsson, S. Kosen, P. Krantz, D. P. Lozano, M. Scigliuzzo, P. Delsing, J. Bylander, and A. Fadavi Roudsari, Appl. Phys. Lett. **118**, 064002 (2021).
[79] A. Bilmes, A. K. Händel, S. Volosheniuk, A. V. Ustinov, and J. Lisenfeld, Supercond. Sci. Technol. **34**, 125011 (2021).
[80] C. Knapp, T. Karzig, R. M. Lutchyn, and C. Nayak, Phys. Rev. B **97**, 125404 (2018).
[81] T. Karzig, W. S. Cole, and D. I. Pikulin, Phys. Rev. Lett. **126**, 057702 (2021).
[82] R.-P. Riwar, A. Hosseinkhani, L. D. Burkhart, Y. Y. Gao, R. J. Schoelkopf, L. I. Glazman, and G. Catelani, Phys. Rev. B **94**, 104516 (2016).

[83] M. Taupin, I. M. Khaymovich, M. Meschke, A. S. Mel'nikov, and J. P. Pekola, Nat. Commun. **7**, 10977 (2016).

[84] L. Tornberg and G. Johansson, Phys. Rev. A **82**, 012329 (2010).

[85] K. Lalumière, J. M. Gambetta, and A. Blais, Phys. Rev. A **81**, 040301(R) (2010).

[86] D. Ristè, M. Dukalski, C. A. Watson, G. de Lange, M. J. Tiggelman, Y. M. Blanter, K. W. Lehnert, R. N. Schouten, and L. DiCarlo, Nature (London) **502**, 350 (2013).

[87] B. Royer, S. Puri, and A. Blais, Sci. Adv. **4**, eaau1695 (2018).

[88] T. Walter, P. Kurpiers, S. Gasparinetti, P. Magnard, A. Potočnik, Y. Salathé, M. Pechal, M. Mondal, M. Oppliger, C. Eichler, and A. Wallraff, Phys. Rev. Applied **7**, 054020 (2017).

[89] R. Dassonneville, T. Ramos, V. Milchakov, L. Planat, É. Dumur, F. Foroughi, J. Puertas, S. Leger, K. Bharadwaj, J. Delaforce, C. Naud, W. Hasch-Guichard, J. J. García-Ripoll, N. Roch, and O. Buisson, Phys. Rev. X **10**, 011045 (2020).

[90] F. Helmer, M. Mariantoni, A. G. Fowler, J. von Delft, E. Solano, and F. Marquardt, Europhys. Lett. **85**, 50007 (2009).

[91] F. Arute *et al.*, Nature (London) **574**, 505 (2019).

[92] A. D. Patterson, J. Rahamim, T. Tsunoda, P. A. Spring, S. Jebari, K. Ratter, M. Mergenthaler, G. Tancredi, B. Vlastakis, M. Esposito, and P. J. Leek, Phys. Rev. Applied **12**, 064013 (2019).

[93] Y. Y. Gao, M. A. Rol, S. Touzard, and C. Wang, PRX Quantum **2**, 040202 (2021).

[94] P. Zhao, D. Lan, P. Xu, G. Xue, M. Blank, X. Tan, H. Yu, and Y. Yu, Phys. Rev. Applied **16**, 024037 (2021).

[95] S. Bravyi, B. M. Terhal, and B. Leemhuis, New J. Phys. **12**, 083039 (2010).